NANO LETTERS

pubs.acs.org/NanoLett Letter

Diffusion-Dominated Luminescence Dynamics of $CsPbBr_3$ Studied Using Cathodoluminescence and Microphotoluminescence Spectroscopy

Sho Nekita, Sotatsu Yanagimoto, Takumi Sannomiya, Keiichirou Akiba, Masato Takiguchi, Hisashi Sumikura, Itsuki Takagi, Kazutaka G. Nakamura, SenPo Yip, You Meng, Johnny C. Ho, Tetsuya Okuyama, Mitsuhiro Murayama, and Hikaru Saito*

Cite This: *Nano Lett.* 2024, 24, 3971−3977 Read Online

ACCESS | Metrics & More | Article Recommendations | Supporting Information

ABSTRACT: Time-resolved or time-correlation measurements using cathodoluminescence (CL) reveal the electronic and optical properties of semiconductors, such as their carrier lifetimes, at the nanoscale. However, halide perovskites, which are promising optoelectronic materials, exhibit significantly different decay dynamics in their CL and photoluminescence (PL). We conducted time-correlation CL measurements of $CsPbBr_3$ using Hanbury Brown-Twiss interferometry and compared them with time-resolved PL. The measured CL decay time was on the order of subnanoseconds and was faster than PL decay at an excited carrier density of 2.1×10^{18} cm^{-3}. Our experiment and analytical model revealed the CL dynamics induced by individual electron incidences, which are characterized by highly localized carrier generation followed by a rapid decrease in carrier density due to diffusion. This carrier diffusion can play a dominant role in the CL decay time for undoped semiconductors, in general, when the diffusion dynamics are faster than the carrier recombination.

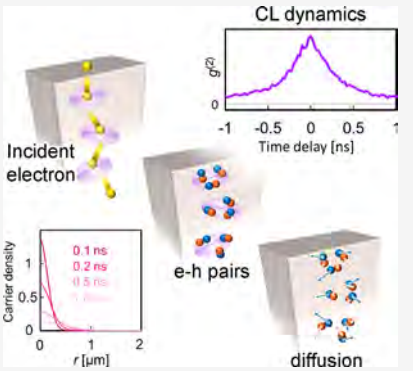

KEYWORDS: *halide perovskite, carrier dynamics, carrier diffusion, cathodoluminescence, photoluminescence, lifetime measurement*

Halide perovskites are promising optoelectronic materials that enable highly efficient solar cells[1] and light-emitting diodes (LEDs).[2] As with other optoelectronic materials, maximizing their performance in practical devices requires nanoscale or atomic scale structural modification such as passivation processes for carrier trapping at interfaces[3] and grain boundaries.[4] The efficiencies of halide perovskite LEDs are dramatically improved by nanoscale coating.[5−7] To analyze the electronic and optical properties of such perovskite materials, cathodoluminescence (CL) combined with electron microscopy has attracted great attention in recent years as a powerful tool that allows local analysis far beyond the diffraction limit of light.[8] In addition to spectroscopic analysis, time-resolved[9,10] or time correlation CL[11−17] offers access to the carrier lifetime at the nanoscale, which is not accessible by conventional photoluminescence (PL) approaches. These advanced CL methods with high spatiotemporal resolution, which enable evaluation of the intrinsic material properties and other nanoscale environmental factors such as the Purcell effect,[13,14] give more comprehensive understanding of the light emission processes, leading to improvements in the efficiencies and operating speeds of optoelectronic devices.

However, the luminescence decay of halide perovskites measured by time-resolved CL in some previous studies[18,19] is obviously faster than that of time-resolved PL (TRPL).[20−22] Although this contradiction suggests that the locality of carrier excitation, which is the crucial difference between CL and PL, can affect emission dynamics, to the best of our knowledge, this point has not been studied.

To clarify the origin of this difference between CL and PL, we conducted time-correlation measurements of CL from $CsPbBr_3$, one of the most widely studied halide perovskites, and compared them with those of TRPL. For the time correlation CL experiments, we employ Hanbury Brown-Twiss (HBT) interferometry,[11−14,17] which does not require a pulsed electron source. The measured CL decay time was on the order of subnanoseconds and was faster than the PL decay at an excited carrier density of 2.1×10^{18} cm^{-3}. On the basis of these experimental results, we introduce a model that considers the locality of carrier excitation and explains the different dynamics of CL and PL.

For doped semiconductors, CL and PL exhibit similar decay dynamics, where the total recombination rate is proportional

Received: January 28, 2024
Revised: March 13, 2024
Accepted: March 14, 2024
Published: March 19, 2024

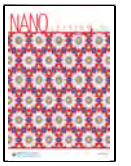

https://doi.org/10.1021/acs.nanolett.4c00483
Nano Lett. 2024, 24, 3971−3977

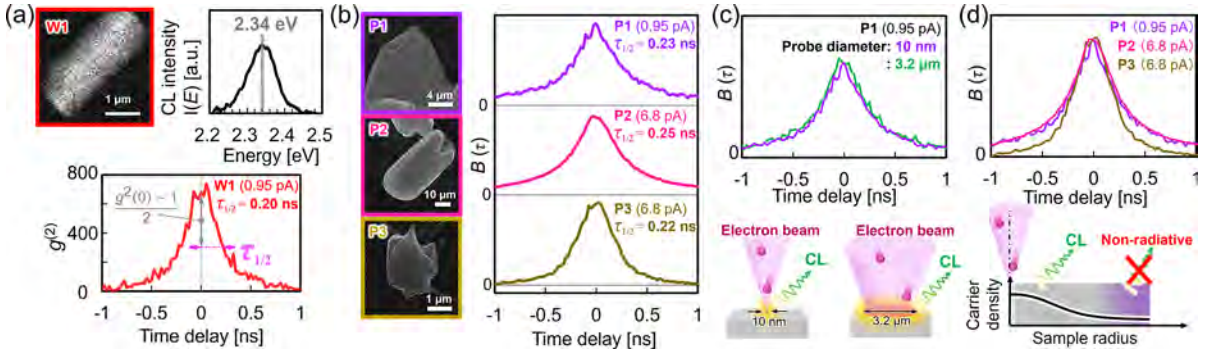

Figure 1. (a) Panchromatic CL image of a CVD-microwire with a thickness of 1.5 μm, CL spectrum $I(E)$, and $g^{(2)}(\tau)$ curve of the microwire (W1). (b) Secondary electron images and $B(\tau)$ curves of ITC-particles (P1, P2, and P3). (c) $B(\tau)$ curves obtained from sample P1 with probe diameters of ~10 nm (purple) and 3.2 μm (green), and a schematic of each irradiation condition. (d) Superposition of $B(\tau)$ curves obtained from the ITC-particles, and a schematic of nonradiative recombination at the surface.

to the density of the excited carrier density, resulting in exponential luminescence decay, characterizing the "one-body" system.[23−25] On the other hand, halide perovskites are typically undoped,[18−22] and the densities of excess electrons and holes become equivalent. The recombination rate is expressed by the following equation, including a quadratic term (two-body effect).[20,21,26,27]

$$\frac{dn}{dt} = -k_1 n - k_2 n^2 \tag{1}$$

Here n is the carrier density, and k_1 and k_2 are material-specific rate coefficients. The second term (two-body effect) causes the decay curve to be nonexponential and the luminescence decay time to be dependent on the excited carrier density. Such an excited carrier density dependence has been observed in halide perovskites by time-resolved PL, and the decay curves follow eq 1.[20,21] Furthermore, the dynamic carrier density decreases because of carrier diffusion, which can affect the resultant luminescence decay through the two-body effect. In fact, a two-dimensional transient absorption microscopy study proposed that such a diffusion effect should be considered when using a highly focused excitation probe.[28] This diffusion effect should be more pronounced in the CL because an electron beam is much smaller than the light probe. Thus, we introduce a diffusion term into the rate equation in the same manner as in the previous study:[28]

$$\frac{dn}{dt} = -k_1 n - k_2 n^2 + D\left[\frac{d^2 n}{dr^2} + \frac{1}{r}\frac{dn}{dr}\right] \tag{2}$$

Here the third term represents the two-dimensional radial diffusion from the excitation position at the coordinate origin, assuming that a focused beam penetrates a thin sample. D is the carrier diffusion coefficient. In the following analysis, we use literature values for $CsPbBr_3$, namely $D \sim 1$ cm^2 s^{-1},[21,29] $k_1 = (2.1 \pm 1.7) \times 10^7$ s^{-1}, and k_2 $(5.7 \pm 2.3) \times 10^{-10}$ cm^3 s^{-1}.[21]

For the experiment, we prepared single-crystal $CsPbBr_3$ microwires by chemical vapor deposition (CVD) on a SiO_2/Si substrate,[30] and polycrystalline $CsPbBr_3$ particles of several micrometers or larger by an inverse temperature crystallization (ITC) method (Supporting Information A).[31−34] None of the prepared $CsPbBr_3$ particles were intentionally doped. Hereafter, these $CsPbBr_3$ samples are referred to as CVD-microwires and ITC-particles, respectively.

We measured CL from the $CsPbBr_3$ samples under electron irradiation with a kinetic energy of 80 keV and probe current values of 0.95 and 6.8 pA at room temperature. The details of the experimental setup are described in Supporting Information B.[14,17] Figure 1a shows a panchromatic image of a fabricated CVD-microwire with a thickness of 1.5 μm (W1), the CL spectrum $I(E)$, and the second-order autocorrelation function $g^{(2)}(\tau)$ curve obtained from this microwire. We confirmed that all of the fabricated CVD-microwires had square cross sections perpendicular to the long axis. The CL spectrum $I(E)$ showed a peak at 2.34 eV. This energy value agrees well with that reported previously, and this peak can be attributed to interband transition.[35,36] This is also supported by UV−vis absorption spectroscopy conducted on an ensemble of numerous CVD-microwires on a SiO_2/Si substrate with an illumination spot of several millimeters. The measured average bandgap energy was 2.32 eV, which is consistent with the observed CL peak (see Supporting Information C and refs 36−38 therein). The decay of this luminescence is reflected in $g^{(2)}(\tau)$[11−14] with photon bunching ($g^{(2)}(\tau) > 1$). To evaluate the emission decay time, we adopted the half-width at half-maximum of the bunching peak, $\tau_{1/2}$, i.e., the period during which the emission rate decreases to half of its initial value. The measured $\tau_{1/2}$ of 0.2 ns was much shorter than $\tau_{1/2}$ of the previously reported TRPL result of about 1 ns obtained at a relatively high photocarrier density (7×10^{17} cm^{-3}).[21] Note that the true $\tau_{1/2}$ value can be even smaller than 0.2 ns if we consider the broadening effect due to the instrument response function (IRF) (Supporting Information B). Figure 1b shows the results of the HBT-CL experiment for three ITC-particles (P1, P2, and P3) obtained with a probe current of 0.95 pA for P1, and 6.8 pA for P2 and P3. For comparison, the obtained $g^{(2)}(\tau)$ curves were normalized as follows:

$$B(\tau) = \frac{g^{(2)}(\tau) - 1}{g^{(2)}(0) - 1} \tag{3}$$

All the CL bunching peaks showed subnanosecond decays regardless of the differences in the synthesis method, the size and shape of the particles, or the probe current. Notably, these subnanosecond CL decays cannot be attributed to defects introduced by electron-beam irradiation because no decrease in the CL intensity was observed during the experiments. The used probe current values of 0.95 and 6.8 pA correspond to the electron incidences with the average time intervals of 170 and 24 ns, respectively. Since these average intervals are much longer than the measured $\tau_{1/2}$, the observed subnanosecond

https://doi.org/10.1021/acs.nanolett.4c00483
Nano Lett. 2024, 24, 3971−3977

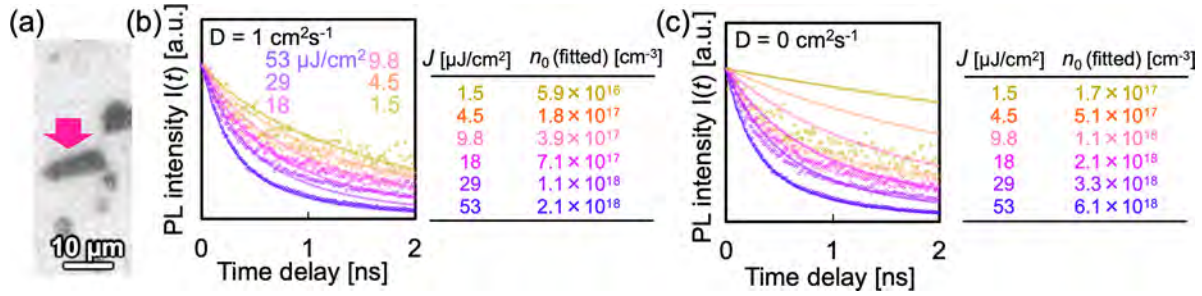

Figure 2. (a) Optical microscope image of a CVD-microwire with a thickness of 4.5 μm. (b, c) Experimental PL intensity $I(t)$ (dots) obtained at several J values, and fitting curves based on (b) eq 2 and (c) eq 1. For the fitting, k_1 and k_2 were set to 2.1×10^7 s^{-1} and 5.7×10^{-10} cm^3 s^{-1}, respectively.[21] The diffusion constant D was set to 1 cm^2 s^{-1} in (b).[21,29] The best fitting set r_0 is 1.0 μm in (b). PL intensity $I(t)$ is normalized by $I(0)$. The fitted values of n_0 are given on the right side of each plot.

CL decays originate from individual electron incidence. This interpretation of the excitation by individual electrons is also supported by the CL decays obtained with different probe diameters of ~10 nm and 3.2 μm at the same probe current value 0.95 pA showing identical CL decays (Figure 1c). While all of the $B(\tau)$ curves are similar up to 0.1 ns, sample P3 decays faster than the others after 0.1 ns (Figure 1d). This acceleration of the CL decay in the relatively small P3 particle can be explained by carrier diffusion to the surface with a high concentration of nonradiative recombination centers.[5,6,21] On the other hand, the $B(\tau)$ curves obtained from samples P1 and P2 with sizes of several micrometers or more show good agreement. Considering the large size difference between P1 and P2, we were concerned that reabsorption effects might cause the carrier generation depth dependence of the CL spectrum.[8] Nevertheless, this effect on the CL dynamics is not observed under our experimental conditions. This is probably because the particles measured are too small to cause significant reabsorption. The particle size-independent decay curve means that CL dynamics in the bulk is observed, and fast phenomena in the bulk shorten the CL decay time. Assuming that the observed CL decay (Figure 1) can be explained by eq 1, the initial carrier density n_0 excited by individual 80 keV electrons should reach an order of 10^{18} cm^{-3} based on the measured values $\tau_{1/2}$ = 0.20−0.25 ns (Supporting Information D). This high carrier density seems overestimated because it is even higher than the carrier density generated by a pulsed electron beam containing 490 electrons per pulse.[39]

We subsequently considered the influence of carrier diffusion on the luminescence dynamics using eq 2. Before applying eq 2 to the discussion of CL dynamics, we evaluate the validity of eq 2 using a micro-TRPL experiment with a focused excitation laser. This micro-TRPL experiment can clarify the carrier density dependence of the luminescence decay by varying the excitation energy density per pulse J. By fitting the decay curves of the series of measurements with varying J, it is possible to determine the initial photocarrier density n_0 and probe radius r_0 in eq 2. A CVD-microwire with a thickness of 4.5 μm shown in Figure 2a was irradiated by a pulsed laser with photon energy of 3.31 eV and a duration of 0.2 ns at room temperature. The details of the experimental setup are described in Supporting Information E. Figure 2b shows the micro-PL decay measured at several different J values. The decay became faster as J, that is, as n_0, increased. Such n_0-dependent decay is characteristic of many-body systems. The experimental micro-PL intensity decay curves $I(t)$ are well reproduced by the theoretical curves obtained by numerically solving eq 2 and integrating the radiative contribution from the detection area:

$$I(t) \propto 2\pi k_2 \int_0^{r_d} \{n(r, t)\}^2 r \, dr \tag{4}$$

Here r_d (=0.9 μm in this experiment) is the radius of the light detection area. Therefore, the observed PL dynamics can be described as a composite system of one- and two-bodies with equal excess electron and hole densities. Since the local photon emission rate for undoped semiconductors is proportional to the square of the photocarrier density n (two-body effect), which has a spatial distribution, the total intensity $I(t)$ is influenced by the carrier diffusion. In this fitting (Supporting Information G), we opted for optimal values of n_0 and r_0 so that the mean squared error (MSE) was minimized between all experimental and theoretical curves, setting the parameter n_0 linear to J. The derived value for r_0 of 1.0 μm is reasonable for the design of the optical system. In contrast, without carrier diffusion reasonable fitting parameters could not be found, especially under low n_0 conditions (Figure 2c). This indicates that carrier diffusion is essential for luminescence decay. While in the current analysis we employ the diffusion coefficient of D = 1 cm^2 s^{-1},[21,29] this MSE analysis has shown that different values, such as D = 2 cm^2 s^{-1},[22] increased the error by a factor of 1.4 (Supporting Information G). Hereafter, we employ D = 1 cm^2 s^{-1}.[21,29] This validates our choice of the initial diffusion coefficient. The temporal evolution of the carrier density distribution calculated for $n_0 = 5.9 \times 10^{16}$ cm^{-3} is shown in Supporting Information F, directly indicating that the carrier diffusion is never negligible when the carrier generation volume is considerably small. We further confirmed that Auger recombination term $k_3 n^3$ (three-body effect)[40] and other many-body effects are negligible in the aforementioned photocarrier density range of the order of 10^{18} cm^{-3} or less (Supporting Information H). Notably, the above results do not completely rule out exciton emission (another one-body effect) in the micrometer-sized $CsPbBr_3$ particle, which was ignored in the analysis. Nevertheless, the possible exciton component does not significantly affect the interpretation because the lifetime of exciton is expected to be longer than 10 ns based on the reported exponential components.[21,22]

The carrier diffusion effect should be more pronounced in CL than in micro-PL, because the carrier generation volume in CL is fundamentally narrower. To apply eq 2 to the HBT-CL results, the individual incident electrons were assumed to travel along the central axis of the cylindrical coordinate system (Figure 3a). The electron−hole pair generation by an electron

https://doi.org/10.1021/acs.nanolett.4c00483
Nano Lett. 2024, 24, 3971−3977

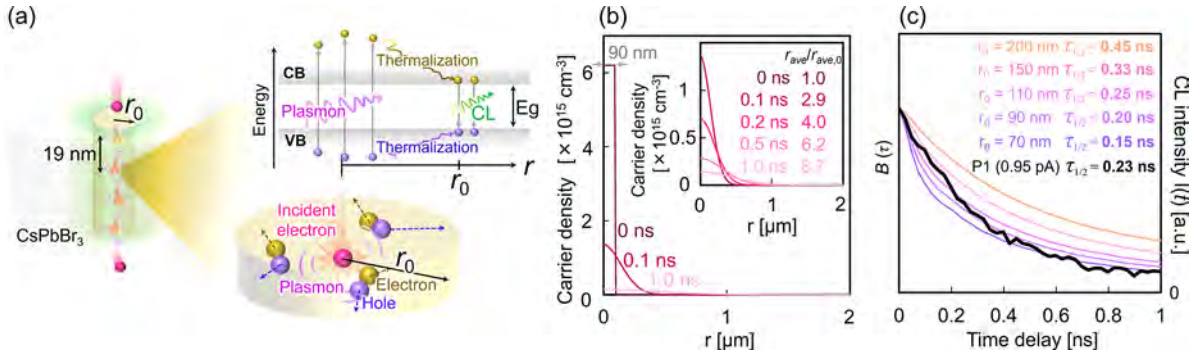

Figure 3. (a) Schematic illustration of the carrier generation process by electron irradiation. r_0 was defined as the initial radius of the radiative recombination which the induced carriers reach by the end of the thermalization process. (b) Temporal evolution of carrier density distribution calculated based on eq 2. r_0 is set to 90 nm. The rate constants k_1, k_2, and diffusion constant D are the same as those in calculations in Figure 2b. The ratio of r_{ave} to the initial value ($r_{ave,0}$) is shown in the inset. (c) Calculated decay $I(t)$ of CL for several r_0 and the experimental $B(\tau)$ curve for sample P1. The IRF for HBT-CL is convoluted in the calculated curves.

beam is mainly mediated by bulk plasmons[41,42] with a decay length of several tens of nanometers.[43] The electron energy-loss spectroscopy (EELS) measurement showed that the single excitation energy of bulk plasmons in $CsPbBr_3$ is 18 eV (see Supporting Information I and refs 44−47 therein). As shown by the trajectory simulation (Supporting Information I) generated using Casino software,[48] most of the incident electrons lose all their kinetic energy (80 keV) before reaching the depth of 25 μm, which is approximately the size of sample P2 in Figure 1. More than 98% of the carriers were generated during the deceleration of incident electrons from 80 to 1 keV. Within this kinetic energy range of the electron beam, the average interval of bulk plasmon excitations was estimated to be 1.5−19 nm by the Bethe formula[49] under the assumption that all inelastic scattering events are accompanied by bulk plasmon excitations. The generation efficiency of electron−hole pairs 0.15−2 nm^{-1} was roughly estimated by assuming three electron−hole pairs are generated per bulk plasmon.[41] The uniform carrier distribution in the cylinder with r_0 was tentatively assumed as the initial carrier distribution for the recombination process. Figure 3b shows the theoretical temporal evolution of the carrier distribution for D = 1 cm^2 s^{-1}, where r_0 = 90 nm was chosen based on the comparison of the experimental $B(\tau)$ obtained from sample P1 and the CL decay curves $I(t)$ calculated for several r_0 values (Figure 3c). For r_0 = 90 nm, the initial carrier density n_0 is on the order of 10^{15} cm^{-3} at the electron beam energy of 80 keV. n_0 increases on the order of 10^{16} cm^{-3} with the deceleration of the incident electrons to 1 keV in the sample. Nevertheless, the calculation at 1 keV shows almost the same CL decay (Supporting Information I), indicating that the carrier increase due to the deceleration of the incident electrons is not sufficient for the second term (radiative recombination) in eq 2 to exceed the dominant contribution of the third term (carrier diffusion). Although this initial carrier density in CL (10^{15} cm^{-3}) is much lower than that in the above micro-TRPL experiment (~10^{16}−10^{18} cm^{-3}), the CL decay is faster. Indeed, carrier diffusion plays a dominant role in CL decay. We define the average radius of the carrier density distribution as follows:

$$r_{ave} = \frac{\int_0^\infty n(r, t) r^2 \, dr}{\int_0^\infty n(r, t) r \, dr} \quad (5)$$

The ratio of r_{ave} to its initial value $r_{ave,0}$ ($r_{ave}/r_{ave,0}$) increases to 8.7 in just 1 ns; that is, the carrier density drops to less than a few % of the initial density within 1 ns (Figure 3b). Accordingly, we concluded that the subnanosecond decay observed in the HBT-CL experiment is due to the carrier diffusion accompanied by a drop in carrier density, and carrier diffusion intrinsically dominates the CL decay because of the narrow carrier generation volume compared to the carrier diffusion range. Notably, the calculated carrier diffusion is less than a few μm within 1 ns. This is supported by the absence of the surface nonradiative recombination in the CL decay curves obtained from samples P1 and P2 (Figure 1d). We do not have to consider the propagation of bulk plasmons for the estimated value of r_0 = 90 nm, which is too long for the plasmon propagation.[43] We emphasize that r_0 is the radius of the cylinder along a single trajectory (Figure 3a) rather than the size of the pear-shaped volume given by a large number of electron trajectories (e.g., Figure S13 in Supporting Information I). Near the end of each trajectory, the cylindrical diffusion model can fail due to frequent and sharp bends in the trajectory as well as a steep carrier density gradient along the trajectory due to deceleration (Figure S13). However, the influence of such irregularities near the end of each trajectory was not observed as understood by the fact that the $B(\tau)$ curves obtained from samples P1 and P2 agree well (Figure 1d) despite largely different decelerations due to their size difference. Possible reasons are that emitted light from such a deep position is reabsorbed, or the position is out of focus of the CL detection optics, or the contribution of such irregularities is too small. We consider that fast electron-induced carriers have high kinetic energy and immediately diffuse during the thermalization process until they reach the bottom of the conduction band or the top of the valence band. This hot-carrier diffusion broadens the carrier distribution before radiative recombination begins (Figure 3a). Hot-carrier generation is possible because the bulk plasmon energy (18 eV) is approximately eight times higher than the bandgap energy (2.32 eV). The local heating through this thermalization process in the CL experiment was estimated to be milder than that in the micro-TRPL experiment (Supporting Information K). Since the micro-TRPL results can also be reasonably reproduced using the parameters determined at room temperature, we can consider that heating by an excitation electron or laser was negligible in the conducted experiments.

https://doi.org/10.1021/acs.nanolett.4c00483
Nano Lett. 2024, 24, 3971−3977

In conclusion, we found a subnanosecond decay of luminescence from $CsPbBr_3$ particles induced by individual 80 keV electrons in the HBT-CL experiment, which was faster than the PL decay at $n_0 = 2.1 \times 10^{18}$ cm^{-3}. We successfully explained this fairly fast CL decay using theoretical modeling, leading to the formulation of diffusion-dominant CL dynamics in $CsPbBr_3$. Each incident electron locally excites carriers at a moderate density of over 10^{15} cm^{-3}, which is, however, highly localized such that the carrier diffusion dominates the decay dynamics through the two-body effect. This diffusion effect is present in both CL and micro-TRPL. In PL, the diffusion effect becomes negligible by increasing the probe size, as seen in the typical TRPL measurement,[21] whereas in CL, it inevitably appears since the highly localized excitation is induced by individual incident electrons. Notably, the diffusion coefficient for $CsPbBr_3$ is moderate among semiconductors (see Supporting Information L and refs 21, 22, 29, 50−66 therein). Therefore, the discrepancy observed between the CL and PL in other halide perovskites[18−21] may be partially or fully explained by eq 2, and the above conclusions can be generalized to the other undoped semiconductors as long as the carrier trapping or excitonic effects are sufficiently small (Supporting Information M). This diffusion-dependent CL decay measurement can be used to evaluate the carrier diffusion constants once the intrinsic emission lifetime is known, for example, using large-probe TRPL. Furthermore, the found carrier diffusion effect offers a new approach for developing fast scintillators that materialize as subnanosecond electron detectors for ultrafast scanning electron imaging.

■ ASSOCIATED CONTENT

Supporting Information

The Supporting Information is available free of charge at https://pubs.acs.org/doi/10.1021/acs.nanolett.4c00483.

Structural analysis, experimental setup, experimental parameters, calculation method, and additional results (PDF)

■ AUTHOR INFORMATION

Corresponding Author

Hikaru Saito − *Department of Materials Science and Engineering, School of Materials and Chemical Technology, Tokyo Institute of Technology, Midoriku, Yokohama 226-8503, Japan; Institute for Materials Chemistry and Engineering, Kyushu University, Kasuga, Fukuoka 816-8580, Japan; Pan-Omics Data-Driven Research Innovation Center, Kyushu University, Fukuoka 816-8580, Japan;* orcid.org/0000-0001-9578-1433; Phone: +81-92-583-7621; Email: saito.hikaru.961@m.kyushu-u.ac.jp

Authors

Sho Nekita − *Interdisciplinary Graduate School of Engineering Sciences, Kyushu University, Kasuga, Fukuoka 816-8580, Japan*

Sotatsu Yanagimoto − *Department of Materials Science and Engineering, School of Materials and Chemical Technology, Tokyo Institute of Technology, Midoriku, Yokohama 226-8503, Japan*

Takumi Sannomiya − *Department of Materials Science and Engineering, School of Materials and Chemical Technology, Tokyo Institute of Technology, Midoriku, Yokohama 226-8503, Japan;* orcid.org/0000-0001-7079-2937

Keiichirou Akiba − *Department of Materials Science and Engineering, School of Materials and Chemical Technology, Tokyo Institute of Technology, Midoriku, Yokohama 226-8503, Japan; Takasaki Institute for Advanced Quantum Science, National Institutes for Quantum Science and Technology (QST), Takasaki, Gunma 370-1292, Japan*

Masato Takiguchi − *Nanophotonics Center, NTT Corp., Atsugi, Kanagawa 243-0198, Japan; NTT Basic Research Laboratories, NTT Corp., Atsugi, Kanagawa 243-0198, Japan;* orcid.org/0000-0001-6294-905X

Hisashi Sumikura − *Nanophotonics Center, NTT Corp., Atsugi, Kanagawa 243-0198, Japan; NTT Basic Research Laboratories, NTT Corp., Atsugi, Kanagawa 243-0198, Japan;* orcid.org/0000-0002-8203-6685

Itsuki Takagi − *Department of Materials Science and Engineering, School of Materials and Chemical Technology, Tokyo Institute of Technology, Midoriku, Yokohama 226-8503, Japan*

Kazutaka G. Nakamura − *Department of Materials Science and Engineering, School of Materials and Chemical Technology, Tokyo Institute of Technology, Midoriku, Yokohama 226-8503, Japan; Laboratory for Materials and Structures, Institute of Innovative Research, Tokyo Institute of Technology, Midoriku, Yokohama 226-8503, Japan*

SenPo Yip − *Institute for Materials Chemistry and Engineering, Kyushu University, Kasuga, Fukuoka 816-8580, Japan*

You Meng − *Department of Materials Science and Engineering, City University of Hong Kong, Kowloon 999077, Hong Kong SAR*

Johnny C. Ho − *Institute for Materials Chemistry and Engineering, Kyushu University, Kasuga, Fukuoka 816-8580, Japan; Department of Materials Science and Engineering, City University of Hong Kong, Kowloon 999077, Hong Kong SAR; State Key Laboratory of Terahertz and Millimeter Waves, City University of Hong Kong, Kowloon 999077, Hong Kong SAR;* orcid.org/0000-0003-3000-8794

Tetsuya Okuyama − *National Institute of Technology, Kurume College, Kurume, Fukuoka 830-8555, Japan*

Mitsuhiro Murayama − *Institute for Materials Chemistry and Engineering, Kyushu University, Kasuga, Fukuoka 816-8580, Japan; Department of Materials Science and Engineering, Virginia Tech, Blacksburg, Virginia 24061, United States;* orcid.org/0000-0003-1965-4891

Complete contact information is available at: https://pubs.acs.org/10.1021/acs.nanolett.4c00483

Notes

The authors declare no competing financial interest.

■ ACKNOWLEDGMENTS

This work was supported by JSPS KAKENHI Grant Number (23KJ1716, 23K17350, 22H05034, 22H01928, 21K18195, 20K21093), Iketani Science and Technology Foundation, Research Foundation for Opto-Science and Technology, and Five-Star Alliance.

■ REFERENCES

(1) Jena, A. K.; Kulkarni, A.; Miyasaka, T. Halide Perovskite Photovoltaics: Background, Status, and Future Prospects. *Chem. Rev.* **2019**, *119*, 3036−3103.

(2) Liu, X. K.; Xu, W.; Bai, S.; Jin, Y.; Wang, J.; Friend, R. H.; Gao, F. Metal halide perovskites for light-emitting diodes. *Nat. Mater.* **2021**, *20*, 10−21.
(3) Feldmann, F.; Simon, M.; Bivour, M.; Reichel, C.; Hermle, M.; Glunz, S. W. Efficient carrier-selective p- and n-contacts for Si solar cells. *Sol. Energy Mater. Sol. Cells* **2014**, *131*, 100−104.
(4) Moseley, J.; Rale, P.; Collin, S.; Colegrove, E.; Guthrey, H.; Kuciauskas, D.; Moutinho, H.; Al-Jassim, M.; Metzger, W. K. Luminescence methodology to determine grain-boundary, grain-interior, and surface recombination in thin-film solar cells. *J. Appl. Phys.* **2018**, *124*, No. 113104.
(5) Li, L.; Hu, Y.; Chen, Y.; Wang, C.; Zhao, G.; Du, X.; Wang, C.; Xiao, L.; Lu, Z.; Wang, J.; Wang, D.; Jie, J.; Huang, J.; Zou, G. Surface Defect Suppression for High Color Purity Light-Emitting Diode of Free-Standing Single-Crystal Perovskite Film. *Adv. Funct. Mater.* **2023**, *33*, No. 2301205.
(6) Lin, K.; Xing, J.; Quan, L. N.; de Arquer, F. P. G.; Gong, X.; Lu, J.; Xie, L.; Zhao, W.; Zhang, D.; Yan, C.; Li, W.; Liu, X.; Lu, Y.; Kirman, J.; Sargent, E. H.; Xiong, Q.; Wei, Z. Perovskite light-emitting diodes with external quantum efficiency exceeding 20%. *Nature* **2018**, *562*, 245−248.
(7) Shi, Z.; Li, Y.; Zhang, Y.; Chen, Y.; Li, X.; Wu, D.; Xu, T.; Shan, C.; Du, G. High-Efficiency and Air-Stable Perovskite Quantum Dots Light-Emitting Diodes with an All-Inorganic Heterostructure. *Nano Lett.* **2017**, *17*, 313−321.
(8) Guthrey, H.; Moseley, J. A Review and Perspective on Cathodoluminescence Analysis of Halide Perovskites Advanced Energy Materials. *Adv. Ener. Mater.* **2020**, *10*, No. 1903840.
(9) Merano, M.; Sonderegger, S.; Crottini, A.; Collin, S.; Renucci, P.; Pelucchi, E.; Malko, A.; Baier, M. H.; Kapon, E.; Deveaud, B.; Ganière, J. D. Probing carrier dynamics in nanostructures by picosecond cathodoluminescence. *Nature* **2005**, *438*, 479−482.
(10) Meuret, S.; Tizei, L. H. G.; Houdellier, F.; Weber, S.; Auad, Y.; Tencé, M.; Chang, H. C.; Kociak, M.; Arbouet, A. Time-resolved cathodoluminescence in an ultrafast transmission electron microscope. *Appl. Phys. Lett.* **2021**, *119*, No. 062106.
(11) Tizei, L. H. G.; Kociak, M. Spatially Resolved Quantum Nano-Optics of Single Photons Using an Electron Microscope. *Phys. Rev. Lett.* **2013**, *110*, No. 153604.
(12) Meuret, S.; Tizei, L. H. G.; Cazimajou, T.; Bourrellier, R.; Chang, H. C.; Treussart, F.; Kociak, M. Photon Bunching in Cathodoluminescence. *Phys. Rev. Lett.* **2015**, *114*, No. 197401.
(13) Lourenco-Martins, H.; Kociak, M.; Meuret, S.; Treussart, F.; Lee, Y. H.; Ling, X. Y.; Chang, H.-C.; Galvao Tizei, L. H. Probing Plasmon-NV^0 Coupling at the Nanometer Scale with Photons and Fast Electrons. *ACS Photonics* **2018**, *5*, 324−328.
(14) Yanagimoto, S.; Yamamoto, N.; Sannomiya, T.; Akiba, K. Purcell effect of nitrogen-vacancy centers in nanodiamond coupled to propagating and localized surface plasmons revealed by photon-correlation cathodoluminescence. *Phys. Rev. B* **2021**, *103*, No. 205418.
(15) Varkentina, N.; Auad, Y.; Woo, S. Y.; Zobelli, A.; Bocher, L.; Blazit, J. D.; Li, X.; Tencé, M.; Watanabe, K.; Taniguchi, T.; Stéphan, O.; Kociak, M.; Tizei, L. H. G. Cathodoluminescence excitation spectroscopy: Nanoscale imaging of excitation pathways. *Sci. Adv.* **2022**, *8*, No. eabq4947.
(16) Yanagimoto, S.; Yamamoto, N.; Yuge, T.; Saito, H.; Akiba, K.; Sannomiya, T. Time-correlated electron and photon counting microscopy. *Commn. Phys.* **2023**, *6*, 260.
(17) Kubota, T.; Yanagimoto, S.; Saito, H.; Akiba, K.; Ishii, A.; Sannomiya, T. Cathodoluminescence spectral and lifetime mapping of Cs_4PbBr_6: fast lifetime and its scintillator application. *Appl. Phys. Exp.* **2024**, *17*, No. 015005.
(18) Ferrer Orri, J.; Tennyson, E. M; Kusch, G.; Divitini, G.; Macpherson, S.; Oliver, R. A; Ducati, C.; Stranks, S. D Using pulsed mode scanning electron microscopy for cathodoluminescence studies on hybrid perovskite films. *Nano Ex.* **2021**, *2*, No. 024002.
(19) Cortecchia, D.; Lew, K. C.; So, J. K.; Bruno, A.; Soci, C. Cathodoluminescence of Self-Organized Heterogeneous Phases in Multidimensional Perovskite Thin Films. *Chem. Mater.* **2017**, *29*, 10088−10094.
(20) Yamada, Y.; Nakamura, T.; Endo, M.; Wakamiya, A.; Kanemitsu, Y. Photocarrier Recombination Dynamics in Perovskite $CH_3NH_3PbI_3$ for Solar Cell Applications. *J. Am. Chem. Soc.* **2014**, *136*, 11610−11613.
(21) Zhu, H.; Trinh, M. T.; Wang, J.; Fu, Y.; Joshi, P. P.; Miyata, K.; Jin, S.; Zhu, X. Y. Organic Cations Might Not Be Essential to the Remarkable Properties of Band Edge Carriers in Lead Halide Perovskites. *Adv. Mater.* **2017**, *29*, No. 1603072.
(22) Yang, B.; Zhang, F.; Chen, J.; Yang, S.; Xia, X.; Pullerits, T.; Deng, W.; Han, K. Ultrasensitive and Fast All-Inorganic Perovskite-Based Photodetector via Fast Carrier Diffusion. *Adv. Mater.* **2017**, *29*, No. 1703758.
(23) Merano, M.; Collin, S.; Renucci, P.; Gatri, M.; Sonderegger, S.; Crottini, A.; Ganière, J. D.; Deveaud, B. High brightness picosecond electron gun. *Rev. Sci. Instrum.* **2005**, *76*, No. 085108.
(24) Chichibu, S. F.; Onuma, T.; Hazu, K.; Uedono, A. Major impacts of point defects and impurities on the carrier recombination dynamics in AlN. *Appl. Phys. Lett.* **2010**, *97*, No. 201904.
(25) Kagaya, M.; Corfdir, P.; Ganière, J. D.; Deveaud-Plédran, B.; Grandjean, N.; Chichibu, S. F. Implementation of Spatio-Time-Resolved Cathodoluminescence Spectroscopy for Studying Local Carrier Dynamics in a Low Dislocation Density m-Plane $In_{0.05}Ga_{0.95}N$ Epilayer Grown on a Freestanding GaN Substrate. *Jpn. J. Appl. Phys.* **2011**, *50*, No. 111002.
(26) Yi, H. T.; Irkhin, P.; Joshi, P. P.; Gartstein, Y. N.; Zhu, X.; Podzorov, V. Experimental Demonstration of Correlated Flux Scaling in Photoconductivity and Photoluminescence of Lead-Halide Perovskites. *Phys. Rev. Applied* **2018**, *10*, No. 054016.
(27) Kim, H.; Shin, D. S.; Ryu, H. Y.; Shim, J. I. Analysis of Time-resolved Photoluminescence of InGaN Quantum Wells Using the Carrier Rate Equation. *Jpn. J. Appl. Phys.* **2010**, *49*, No. 112402.
(28) Guo, Z.; Manser, J. S.; Wan, Y.; Kamat, P. V.; Huang, L. Spatial and temporal imaging of long-range charge transport in perovskite thin films by ultrafast microscopy. *Nat. Commun.* **2015**, *6*, 7471.
(29) Kennedy, C. L.; Hill, A. H.; Grumstrup, E. M. Screening Links Transport and Recombination Mechanisms in Lead Halide Perovskites. *J. Phys. Chem. C* **2019**, *123*, 15827−15833.
(30) Meng, Y.; Lai, Z.; Li, F.; Wang, W.; Yip, S.; Quan, Q.; Bu, X.; Wang, F.; Bao, Y.; Hosomi, T.; Takahashi, T.; Nagashima, K.; Yanagida, T.; Lu, J.; Ho, J. C. Perovskite Core−Shell Nanowire Transistors: Interfacial Transfer Doping and Surface Passivation. *ACS Nano* **2020**, *14*, 12749−12760.
(31) Dirin, D. N.; Cherniukh, I.; Yakunin, S.; Shynkarenko, Y.; Kovalenko, M. V. Solution-Grown $CsPbBr_3$ Perovskite Single Crystals for Photon Detection. *Chem. Mater.* **2016**, *28*, 8470−8474.
(32) Ghosh, G.; Jana, B.; Sain, S.; Ghosh, A.; Patra, A. Influence of shape on the carrier relaxation dynamics of $CsPbBr_3$ perovskite nanocrystals. *Phys. Chem. Chem. Phys.* **2019**, *21*, 19318−19326.
(33) Rakita, Y.; Kedem, N.; Gupta, S.; Sadhanala, A.; Kalchenko, V.; Böhm, M. L.; Kulbak, M.; Friend, R. H.; Cahen, D.; Hodes, G. Low-Temperature Solution-Grown $CsPbBr_3$ Single Crystals and Their Characterization. *Cryst. Growth Des.* **2016**, *16*, 5717−5725.
(34) Di, J.; Li, H.; Su, J.; Yuan, H.; Lin, Z.; Zhao, K.; Chang, J.; Hao, Y. Reveal the Humidity Effect on the Phase Pure $CsPbBr_3$ Single Crystals Formation at Room Temperature and Its Application for Ultrahigh Sensitive X-Ray Detector. *Adv. Sci.* **2022**, *9*, No. 2103482.
(35) Zhao, M.; Shi, Y.; Dai, J.; Lian, J. Ellipsometric study of the complex optical constants of a $CsPbBr_3$ perovskite thin film. *J. Mater. Chem. C* **2018**, *6*, 10450−10455.
(36) Shoaib, M.; Zhang, X.; Wang, X.; Zhou, H.; Xu, T.; Wang, X.; Hu, X.; Liu, H.; Fan, X.; Zheng, W.; Yang, T.; Yang, S.; Zhang, Q.; Zhu, X.; Sun, L.; Pan, A. Directional Growth of Ultralong $CsPbBr_3$ Perovskite Nanowires for High-Performance Photodetectors. *J. Am. Chem. Soc.* **2017**, *139*, 15592−15595.
(37) Tauc, J.; Grigorovici, R.; Vancu, A. Optical Properties and Electronic Structure of Amorphous Germanium. *Phys. Status Solidi* **1966**, *15*, 627−637.

https://doi.org/10.1021/acs.nanolett.4c00483
Nano Lett. 2024, 24, 3971−3977

(38) Coulter, J. B.; Birnie, D. P. Assessing Tauc Plot Slope Quantification: ZnO Thin Films as a Model System. *Phys. Status. Solidi. B* **2018**, *255*, No. 1700393.
(39) Solà-Garcia, M.; Mauser, K. W.; Liebtrau, M.; Coenen, T.; Christiansen, S.; Meuret, S.; Polman, A. Photon Statistics of Incoherent Cathodoluminescence with Continuous and Pulsed Electron Beams. *ACS Photonics* **2021**, *8*, 916−925.
(40) Saba, M.; Cadelano, M.; Marongiu, D.; Chen, F.; Sarritzu, V.; Sestu, N.; Figus, C.; Aresti, M.; Piras, R.; Geddo Lehmann, A.; Cannas, C.; Musinu, A.; Quochi, F.; Mura, A.; Bongiovanni, G. Correlated electron−hole plasma in organometal perovskites. *Nat. Commun.* **2014**, *5*, 5049.
(41) Rothwarf, A. Plasmon theory of electron-hole pair production: efficiency of cathode ray phosphors. *J. Appl. Phys.* **1973**, *44*, 752−756.
(42) Werner, W. S. M.; Ruocco, A.; Offi, F.; Iacobucci, S.; Smekal, W.; Winter, H.; Stefani, G. Role of surface and bulk plasmon decay in secondary electron emission. *Phys. Rev. B* **2008**, *78*, No. 233403.
(43) Manfrinato, V. R.; Wen, J.; Zhang, L.; Yang, Y.; Hobbs, R. G.; Baker, B.; Su, D.; Zakharov, D.; Zaluzec, N. J.; Miller, D. J.; Stach, E. A.; Berggren, K. K. Determining the Resolution Limits of Electron-Beam Lithography: Direct Measurement of the Point-Spread Function. *Nano Lett.* **2014**, *14*, 4406−4412.
(44) Chen, X.; Wang, Y.; Song, J.; Li, X.; Xu, J.; Zeng, H.; Sun, H. Temperature Dependent Reflectance and Ellipsometry Studies on a $CsPbBr_3$ Single Crystal. *J. Phys. Chem. C* **2019**, *123*, 10564−10570.
(45) Egerton, R. F. *Electron Energy-Loss Spectroscopy in the Electron Microscope*; Springer: New York, 2011.
(46) Navas, J.; Sánchez-Coronilla, A.; Gallardo, J. J.; Piñero, J. C.; De los Santos, D.; Martín, E. I.; Hernández, N. C.; Alcántara, R.; Fernández-Lorenzo, C.; Martín-Calleja, J. The impact of Pd on the light harvesting in hybrid organic-inorganic perovskite for solar cells. *Nano Energy* **2017**, *34*, 141−154.
(47) Kiguchi, T.; Wakiya, N.; Shinozaki, K.; Konno, T. J. Valence-EELS analysis of local electronic and optical properties of PMN−PT epitaxial film. *Mater. Sci. Eng., B* **2009**, *161*, 160−165.
(48) Drouin, D.; Couture, A. R.; Joly, D.; Tastet, X.; Aimez, V.; Gauvin, R. CASINO V2.42—A Fast and Easy-to-use Modeling Tool for Scanning Electron Microscopy and Microanalysis Users. *Scanning* **2007**, *29*, 92−101.
(49) Joy, D. C.; Luo, S. An empirical stopping power relationship for low-energy electrons. *Scanning* **1989**, *11*, 176−180.
(50) Sun, N.; Jarasiunas, K.; Sudzius, M.; Kadys, A.; Zhou, X.; Sun, T. Role of deep traps in carrier generation and transport in differently doped InP wafers. *Mater. Sci. Semicond. Process* **2006**, *9*, 390−393.
(51) Rosenwaks, Y.; Shapira, Y.; Huppert, D. Picosecond time-resolved luminescence studies of surface and bulk recombination processes in InP. *Phys. Rev. B* **1992**, *45*, 9108.
(52) Chen, K.; Sheehan, N.; He, F.; Meng, X.; Mason, S. C.; Bank, S. R.; Wang, Y. Measurement of Ambipolar Diffusion Coefficient of Photoexcited Carriers with Ultrafast Reflective Grating-Imaging Technique. *ACS Photonics* **2017**, *4*, 1440.
(53) Jarasiunas, K.; Lovergine, N. Characterisation of bulk crystals and structures by light-induced transient grating technique. *Mater. Sci. Eng.* **2002**, *91*−*92*, 100−104.
(54) Chen, K.; Wang, W.; Chen, J.; Wen, J.; Lai, T. A transmission-grating-modulated pump-probe absorption spectroscopy and demonstration of diffusion dynamics of photoexcited carriers in bulk intrinsic GaAs film. *Opt. Express* **2012**, *20*, 3580−3585.
(55) Ruzicka, B. A.; Werake, L. K.; Samassekou, H.; Zhao, H. Ambipolar diffusion of photoexcited carriers in bulk GaAs. *Appl. Phys. Lett.* **2010**, *97*, No. 262119.
(56) Ščajev, P.; Jarašiūnas, K.; Okur, S.; Özgür, Ü.; Morkoç, H. Carrier dynamics in bulk GaN. *J. Appl. Phys.* **2012**, *111*, No. 023702.
(57) Olaizola, S. M.; Fan, W. H.; Hashemizadeh, S. A.; Wells, J.-P. R.; Mowbray, D. J.; Skolnick, M. S.; Fox, A. M.; Parbrook, P. J. Time-resolved photoluminescence studies of carrier diffusion in GaN. *Appl. Phys. Lett.* **2006**, *89*, No. 072107.
(58) Nargelas, S.; Malinauskas, T.; Kadys, A.; Dimakis, E.; Moustakas, T. D.; Jarašiuūnas, K. Nonlinear carrier recombination and transport features in highly excited InN layer. *Phys. Status Solidi C* **2009**, *6*, S735−S738.
(59) Podlipskas, Z.; Jurkevicius, J.; Kadys, A.; Kolenda, M.; Kovalevskij, V.; Dobrovolskas, D.; Aleksiejunas, R.; Tamulaitis, G. Extreme radiation resistance in InN. *J. Alloys Compd.* **2019**, *789*, 48−55.
(60) Ščajev, P.; Miasojedovas, S.; Mekys, A.; Kuciauskas, D.; Lynn, K. G.; Swain, S. K.; Jarašiūnas, K. Excitation-dependent carrier lifetime and diffusion length in bulk CdTe determined by time-resolved optical pump-probe techniques. *J. Appl. Phys.* **2018**, *123*, No. 025704.
(61) Kuciauskas, D.; Myers, T. H.; Barnes, T. M.; Jensen, S. A.; Motz, A. M. A. Time-resolved correlative optical microscopy of charge-carrier transport, recombination, and space-charge fields in CdTe heterostructures. *Appl. Phys. Lett.* **2017**, *110*, No. 083905.
(62) Kuciauskas, D.; Wernsing, K.; Jensen, S. A.; Barnes, T. M.; Myers, T. H.; Bartels, R. A. Analysis of Recombination in CdTe Heterostructures With Time-Resolved Two-Photon Excitation Microscopy. *IEEE J. Photovolt.* **2016**, *6*, 1581−1586.
(63) Weber, C.; Becker, U.; Renner, R.; Klingshirn, C. Measurement of the diffusion-length of carriers and excitons in CdS using laser-induced transient gratings. *Z. Phys. B* **1988**, *72*, 379−384.
(64) Jarašiūnas, K.; Gerritsen, H. J. Ambipolar diffusion measurements in semiconductors using nonlinear transient gratings. *Appl. Phys. Lett.* **1978**, *33*, 190−193.
(65) Netiksis, V.; Juodkazis, S.; Petrauskas, M.; Honerlage, B.; Levy, R.; Ding, Y. Near band-gap nonlinearities of ZnSe crystals. *Opt. Commun.* **1996**, *126*, 247−250.
(66) Wu, B.; Zhou, Y.; Xing, G.; Xu, Q.; Garces, H. F.; Solanki, A.; Goh, T. W.; Padture, N. P.; Sum, T. C. Long Minority-Carrier Diffusion Length and Low Surface-Recombination Velocity in Inorganic Lead-Free $CsSnI_3$ Perovskite Crystal for Solar Cells. *Adv. Funct. Mater.* **2017**, *27*, No. 1604818.

https://doi.org/10.1021/acs.nanolett.4c00483
Nano Lett. 2024, 24, 3971−3977